used in this study, but it is obvious that other procedures could be employed.

The convergence criterion used was that

$$\sum_i [|\ln f_{iI}/f_{iIII}| + |\ln(f_{iII}/f_{iIII})|] < 1 \times 10^{-4}$$

With this criterion, convergence occurred, at best, with 50 iterations. At worst more than 1000 iterations may be required.

Computations were performed on a CDC 6400. On this machine the computing time was roughly 0.003 sec./iteration per component. As indicated, computing time increases linearly with the number of components.

The advantages of this procedure lie in its ease of formulation and programming, its tie to thermodynamic principles, and its reliability. The formulation presented here can easily be extended to more than three phases which makes it a candidate for use in computations where solid phases need be considered, as in cryogenic applications.

Since the procedure minimizes free energy, it is possible to avoid spurious solutions to the equilibrium problem such as those pointed out in the discussion of Figure 5e. In the liquid-liquid-vapor computations the starting point was that almost all the water was in a water rich liquid with a few percent of the total water being present in the two hydrocarbon rich phases. The hydrocarbons were distributed so that the vapor phase was rich in the light components and the liquid phase was rich in the heavy components. This assured convergence to the correct equilibrium conditions.

*Manuscript received January 31, 1974; revision received May 16 and May 20, 1974.*

# Determination of the Kinetics of Secondary Nucleation in Batch Crystallizers

**The kinetics of secondary nucleation have been determined from measurement of the supersaturation as a function of time following the addition of seed nuclei to a supercooled solution in a well-stirred batch crystallizer. Population balance mathematics have been used to show that the secondary nucleation kinetics may be inferred from the supersaturation-time curve. The method has been applied to the determination of the kinetics of the secondary nucleation of ice and found to give results in excellent agreement with those obtained from tedious particle counts. In addition, it has been shown that the moment of the particle size distribution that best correlates the nucleation rate data can be inferred from the initial transient of the supersaturation-time history.**

**S. G. KANE**
**T. W. EVANS**
**P. L. T. BRIAN**
**and**
**A. F. SAROFIM**

**Department of Chemical Engineering**
**Massachusetts Institute of Technology**
**Cambridge, Massachusetts 02139**

## SCOPE

The use of batch crystallizers for the determination of the kinetics of secondary nucleation is complicated by the variation during an experiment in both the number of crystals and the supersaturation. Motivation for the use of batch crystallizers is provided, however, by the relative ease with which a large range of operational variables may be studied in a short time.

This paper develops techniques for obtaining kinetics of secondary nucleation for one mode of operation of a batch crystallizer. A seed crystal is introduced in a supercooled solution and measurements are made of the variation with time of either the number of crystals or the supersaturation. Up to a critical time, designated here as the induction time, the multiplication in the number of crystals occurs with an insignificant variation in the supersaturation. Measurement of the number of crystals during his period of relatively constant supersaturation provides one method of obtaining nucleation kinetics. Particle counts, however, may be tedious or difficult, particularly for systems such as ice where crystals are relatively unstable. One major objective in this paper is therefore the development of methods for inferring nucleation kinetics from the supersaturation measured at times greater than the induction time.

It should be noted that the inference of nucleation kinetics is complicated by the fact that the rate of secondary nucleation may be proportional to the $n$th moment of the particle size distribution

$$\dot{N} = a_n \mu_n$$

Complete characterization of the nucleation kinetics would therefore require the determination of two parameters $n$ and $a_n$. It will be shown, however, that a single

Correspondence concerning this paper should be addressed to A. F. Sarofim. S. G. Kane is with Amoco Chemicals Corporation, Naperville, Illinois. T. W. Evans is with The Upjohn Company, Kalamazoo, Michigan. P. L. T. Brian is with Air Products Corporation, Allentown, Pennsylvania.

composite parameter of $n$, $a_n$, and the growth rate $G$ can characterize many of the important features of the operation of both batch and continuous crystallizers. Conversely, only the composite parameter ($\beta$) may be inferred from the measurements most frequently made in batch or continuous crystallizers. An added feature of the study then became the design of special experiments to infer $n$ and $a_n$ separately.

The experimental component of the study is restricted to the crystallization of ice from brine. The methodology developed may, however, be applied to the study of secondary nucleation in general.

## CONCLUSIONS AND SIGNIFICANCE

Measurement of crystal count or supersaturation following the seeding of a supercooled solution provides an effective method of measuring the kinetics of secondary nucleation. The kinetic constant may be inferred from the rate of increase of the number of crystals during the initial period of essentially constant supersaturation or from the shape of the supersaturation time curve at longer times. The kinetics of nucleation of ice in saline solution obtained using both methods were found to be in good agreement. The method is, however, restricted to the study of secondary nucleation in dilute crystal suspensions.

The kinetic parameter $\beta$ inferred from the batch experiments is related to the true kinetic constant $a_n$ by $\beta = (n!\ a_n\ G^n)^{1/(n+1)}$. This parameter $\beta$ has been shown to be equal to the nucleation rate per crystal in continuous crystallizers and provides a completely adequate characterization of the nucleation kinetics in continuous mixed suspension mixed product removal crystallizers. A corollary to this conclusion is that the nucleation rate can be correlated equally well using any moment of the particle size distribution because the moments are constant ratios of each other. Values of $n$ and $a_n$ may, however, be inferred from experiments conducted with seeds of known size provided measurements are made at times before the particle size distribution becomes self preserving.

### ANALYSIS OF A BATCH CRYSTALLIZER

The particle balance equation for a batch crystallizer is

$$\frac{\partial f}{\partial t} + \frac{\partial}{\partial r}(Gf) = \dot{N}\psi(r) \tag{1}$$

where $f dr$ is the number of crystals per unit volume in the size range $r$ to $dr$, $G$ is the growth rate ($\partial r/\partial t$), $\dot{N}$ is the nucleation rate per unit volume, and $\psi(r)dr$ is the fraction of crystals born in the size range $r$ to $r + dr$. The first term on the left-hand side represents the change in the number of crystals in the size range $r$ to $r + dr$ as a function of time. The second term is the number of crystals growing into the size range less the crystals growing out of the size range. The final term expresses the number of new crystals nucleated into this size range. Solutions to Equation (1) will be obtained here for the case of constant subcooling. It is assumed that:

1. Growth rate is independent of crystal size
2. New crystals are nucleated at near zero size
3. Nucleation rate is proportional to the $n$th moment of the particle size distribution, that is,

$$\dot{N} = a_n \int_0^\infty r^n f\, dr \equiv a_n \mu_n \tag{2}$$

Applying these assumptions to the population balance results in the following equation:

$$\frac{\partial f}{\partial t} + G\frac{\partial f}{\partial r} = a_n \mu_n \delta(r - 0) \tag{3}$$

where $\delta(r - 0)$ is the Dirac delta function. Multiplying Equation (3) by $r^m$ and integrating with respect to $r$ between the limits 0 to $\infty$*

$$\frac{d\mu_m}{dt} = m\, G\mu_{m-1} + \delta_{om}\, a_n \mu_n \tag{4}$$

where $\delta_{om}$ is the Kronecker delta. For any integer value of $n$, Equation (4) can be rewritten as a set of $(n + 1)$ ordinary differential equations:

$$\begin{aligned} \frac{d\mu_o}{dt} &= a_n \mu_n \\ \frac{d\mu_1}{dt} &= G\mu_o \\ &\vdots \\ \frac{d\mu_n}{dt} &= nG\mu_{n-1} \end{aligned} \tag{5}$$

This set of equations can be combined to yield

$$\frac{d^{n+1}\mu_o}{dt^{n+1}} - \beta^{n+1}\mu_o = 0 \tag{6}$$

where

$$\beta = (n!\ a_n\ G^n)^{1/(n+1)}$$

The initial conditions are given by the zeroth to $n$th moments of the seed particle size distribution. The solutions for $\mu_0$ and $\mu_2$ are presented in Table 1 for values of $n$ from 0 to 3. The first term of the solution is dominant at long times (For $\mu_0$, the higher terms contribute less than 5% when $\beta t$ exceeds 1.5 for $n = 1$, 2.9 for $n = 2$, and 3.7 for $n = 3$). Therefore when $\beta t$ exceeds 2 to 4 depending on $n$, the solution for $\mu_0$ and $\mu_2$ can be adequately approximated by

$$\mu_0 = \frac{\mu_0^0}{n+1}\left(1 + \sum_{k=1}^{n} \delta_k\right)\exp(\beta t) \tag{7}$$

$$\mu_2 = \frac{\mu_0^0}{n+1}\left(1 + \sum_{k=1}^{n} \delta_k\right)(2G^2/\beta^2)\exp(\beta t) \tag{8}$$

where $\mu_0^0$ is the number of seed crystals and $\delta_k$ is defined in Table 1.

* In practice the upper limit is $Gt$ for all crystals other than the seed crystals, but this does not affect the mathematical development.

It should be noted that at long times when the values of the moments are dominated by the term growing exponentially with $\beta t$, the ratios of the moments become constant and therefore the particle size distribution becomes self-preserving. This conclusion is based here on an analysis for growth rates independent of crystal size; however, this conclusion is shown in Appendix A to be equally valid for size dependent growth rates.

Equation (8) which describes the increase in surface area of the ice crystals may be combined with an enthalpy balance on the crystallizer to obtain a description of the transient temperature change. Although the methodology developed is applicable to any secondary nucleation process, the discussion that follows will be restricted to the secondary nucleation of ice because of the authors' interest in the freezing process for desalination. It is assumed that the ice crystals are disk-shaped with radius $r$ and width $2h$ and that the aspect ratio $r/h$ is independent of crystal size. The latter assumption is equivalent to requiring that the ratio of growth rates of the $a$ and $c$ axes of ice, $G_a/G_c$, be equal to $r/h$. The time-rate of change of the volume $V_c$ of a crystal of size $r$ is then given by

$$\frac{dV_c}{dt} = \frac{d}{dt}(2\pi r^2 h) = 2\pi r^2\left(\frac{dh}{dt} + 2\frac{h}{r}\frac{dr}{dt}\right)$$

$$= 2\pi r^2\left(G_c + 2\frac{G_c}{G_a}G_a\right) = 6\pi r^2 G_c \quad (9)$$

The volumetric rate of ice production, per unit volume of crystallizer, is the frequency weighted mean of Equation (9), or

$$\int_0^\infty f\frac{dV_c}{dt}\,dr = 6\pi\mu_2 G_c \quad (10)$$

This result may be used in an enthapy balance to yield

$$\rho C_p\frac{dT}{dt} = 6\pi\mu_2 G_c\lambda\rho_I \quad (11)$$

where $\lambda$ is the latent heat of fusion of ice, $\rho C_p$ the density-specific heat product for the liquid, and $\rho_I$ the density of ice. Combining Equation (8) and (11) yields

$$\frac{dT}{dt} = \frac{6\pi\lambda\rho_I}{\rho C_p}\frac{\mu_0^0}{n+1}\left(1 + \sum_{k=1}^{n}\delta_k\right)\frac{2G_a^2 G_c}{\beta^2}\exp\beta t \quad (12)$$

The above analysis suggests that the parameter $\beta$ may be determined either from the total count of the crystals vs. time, using Equation (7), or from the temperature transient, Equation (12). Both techniques were used in this study.

The real question to be resolved is how $\beta$ is related to the nucleation rate. The population balance for a continuous crystallizer at steady state will be solved under the same assumptions that were employed in the solution of Equation (1). The resulting particle size distribution $f$ and the moments of this distribution $\mu_m$ are given by

$$f = f_0\exp(-r/G\tau) \quad (13)$$

TABLE 1. NUMBER OF CRYSTALS AND SECOND MOMENT OF PARTICLE SIZE DISTRIBUTION FOR DIFFERENT NUCLEATION LAWS $\dot{N} = a_n\mu_n$

A. Number of crystals $\equiv \mu_0$

$n$

0 $\mu_0 = \mu_0^0\exp(\beta t)$

1 $\mu_0 = (1/2\,\mu_0^0)\,[(1+\delta_1)\exp(\beta t) + (1-\delta_1)\exp(-\beta t)]$

2 $\mu_0 = (1/3\,\mu_0^0)\left\{(1+\delta_1+\delta_2)\exp(\beta t) + \left[\begin{array}{l}(2-\delta_1-\delta_2)\cos\left(\frac{\sqrt{3}}{2}\beta t\right)\\ +(-\sqrt{3}\delta_1+\sqrt{3}\delta_2)\sin\left(\frac{\sqrt{3}}{2}\beta t\right)\end{array}\right]\exp\left(-\frac{\beta}{2}t\right)\right\}$

3 $\mu_0 = (1/4\,\mu_0^0)\{(1+\delta_1+\delta_2+\delta_3)\exp(\beta t) + (1-\delta_1+\delta_2-\delta_3)\exp(-\beta t)$
$+ [(2-2\delta_2)\cos(\beta t) + (-2\delta_1+2\delta_3)\sin(\beta t)]\}$

B. Second Moment of Particle Size Distribution $\equiv \mu_2$

$n$

0 $\mu_2 = \left(\frac{2G^2}{\beta^2}\right)\mu_0^0\,[\exp(\beta t) + (-1+\delta_1)(\beta t) + (\delta_2 - 1)]$

1 $\mu_2 = \left(\frac{2G^2}{\beta^2}\right)(1/2\,\mu_0^0)\,[(1+\delta_1)\exp(\beta t) + (1-\delta_1)\exp(-\beta t) + 2(\delta_2-1)]$

2 $\mu_2 = \left(\frac{2G^2}{\beta^2}\right)(1/3\,\mu_0^0)\left\{(1+\delta_1+\delta_2)\exp(\beta t) + \left[\begin{array}{l}(-1-\delta_1+2\delta_2)\cos\left(\frac{\sqrt{3}}{2}\beta t\right)\\ +(-\sqrt{3}+\sqrt{3}\delta_1)\sin\left(\frac{\sqrt{3}}{2}\beta t\right)\end{array}\right]\exp\left(-\frac{\beta}{2}t\right)\right\}$

3 $\mu_2 = \left(\frac{2G^2}{\beta^2}\right)(1/4\,\mu_0^0)\{(1+\delta_1+\delta_2+\delta_3)\exp(\beta t) + (1-\delta_1+\delta_2-\delta_3)\exp(\beta t)$
$+ [(-2+2\delta_2)\cos(\beta t) + (2\delta_1-2\delta_3)\sin(\beta t)]\}$

where, in general, $\delta_k = \left(\frac{\mu_k^0}{\mu_0^0}\right)\Big/\left(\frac{(k!)\,G^k}{\beta^k}\right) = \frac{k\text{th moment of seed crystal PSD}}{k\text{th moment of self preserving PSD}}$

and

$$\mu_m \equiv \int_0^\infty r^m f(r)\,dr = f_0\Gamma(m+1)(G\tau)^{m+1} \quad (14)$$

where $f_0$ is the value of $f$ at $r = 0$ and $\tau$ is the mean residence time. From a crystal balance at steady state the nucleation rate in the crystallizer can be equated to the rate of withdrawal of crystals in the effluent from the crystallizer, or

$$\frac{\dot{N}}{\mu_0} = \frac{a_n\mu_n}{\mu_0} = \frac{1}{\tau} \quad (15)$$

combining Equations (14) and (15) yields

$$a_n(n!)(G\tau)^n = 1/\tau$$

or, on rearrangement

$$\beta = \frac{1}{\tau} = [(n!)a_nG^n]^{1/(n+1)} \quad (16)$$

From the right-hand side of Equation (16) and reference to the definition of $\beta$ after Equation (6) it will be noted that $\beta$ is the nucleation rate per crystal. $\beta$ also is equal to the inverse of the average residence time in a continuous MSMPR crystallizer. It is important to make the distinction between the actual nucleation rate $N$ and the nucleation rate per crystal $\beta$, which are related by Equation (15). The relationship between the actual nucleation rate constant $a_n$ and $\beta$ is demonstrated in Equation (16). In order to calculate $a_n$, given $\beta$, it is necessary to know the dependency of the actual nucleation rate on the crystal size $n$ and the crystal growth rate. While $a_n$ and $n$ are more fundamental parameters, $\beta$ is the parameter of importance in continuous MSMPR crystallizers and is easier to measure. $a_n$ and $n$ need to be known, however, for modeling the initial transient in a batch crystallizer and the dynamics of continuous crystallizers.

From Equation (13) the crystal size distribution in a continuous MSMPR crystallizer can be completely characterized by two variables ($G/\beta$ and $f_0$). Since the mass of the crystals is proportional to the third moment of the crystal size distribution which can be calculated from Equation (14), $f_0$ can be related to the ratio $G/\beta$ and the total mass of crystals in the crystallizer. Thus the crystal size distribution can be fully characterized by the ratio of the crystal growth rate to the nucleation rate per crystal and the total mass of crystals. Since the crystal size distribution is uniquely characterized by these two variables, only two variables can be determined from the CSD (crystal size distribution) of an experiment performed in an unseeded continuous MSMPR crystallizer operated at steady state. By measuring the average residence time it is possible to obtain a third variable $\beta$. Even so, $\beta$ is a function of both $a_n$ and $n$, and thus it is not possible to completely characterize the nucleation rate by such an experiment. Methods of inferring $a_n$ and $n$ from the initial transient of a batch experiment, in addition to obtaining the composite parameter $\beta$, are developed in this paper.

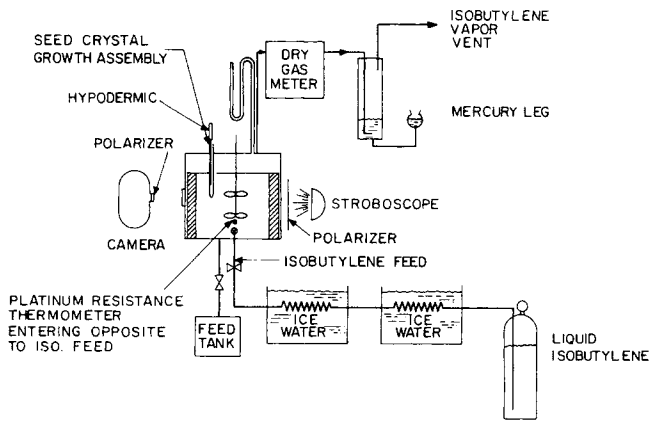


Fig. 1. Schematic diagram of apparatus.

## EXPERIMENT

A flow diagram of the apparatus is shown in Figure 1. The crystallizer was fabricated from an 0.18 m I.D., plastic cylinder, 0.20 m in length. Two circular plastic plates served as covers at the top and at the bottom. The crystallizer was lagged with 0.013 m Armaflex insulation on the sides and at the top. The agitator shaft passed through an 'O' ring seal in the center of the top cover and was connected to a ¼ HP motor through a variable speed 0-300 RPS hydraulic drive. Agitation was provided either by a pair of downward pumping marine propellors or a radially mixing turbine. The marine propellors each had a diameter of 0.069 m and a pitch of 0.103 m and their center planes were positioned 0.053 m apart with the top plane of the lower 0.038 m from the bottom of the crystallizer. The six-bladed turbine with 0.02 m wide flat-blades was 0.102 m in diameter and was positioned with its disk plane 0.032 m above the crystallizer bottom. The crystallizer contained four equally spaced baffles which were 0.019 m wide and positioned 0.013 m from the cylinder wall.

The feed consisted of $3 \times 10^{-3}$ m$^3$ of either tap water or saline solutions cooled to near freezing by means of an auxiliary glycol refrigeration system. The solution temperature was measured with a thermistor bead which yielded temperature readings within ±0.001°K. The thermistor was inserted through the side 0.051 m from the bottom of the crystallizer.

Retrigeration was provided by liquid isobutylene precooled to 0°C. The isobutylene was dispersed through four orifices ($2 \times 10^{-4}$ m dia.) bored into two $0.32 \times 10^{-2}$ m stainless steel tubes. The orifices were equally spaced in a circle of 0.1 m diameter and were positioned 0.013 m from the crystallizer bottom.

After vaporizing in the crystallizer, the isobutylene was withdrawn through the top cover of the crystallizer, passed through a dry gas meter, and then discharged to the exhaust duct through a column of mercury. The isobutylene boiling point and hence the refrigerant subcooling was determined by the crystallizer pressure, which was regulated by adjusting the height of the mercury column.

In a typical experiment, ice crystals in a small volume element of the crystallizer were recorded cinematographically with a 16 mm camera sighted through a glass window on the side of the crystallizer. Back lighting was provided by a stroboscope having a flash duration of $10^{-6}$ s. Sufficient contrast between the ice crystals and the solution was obtained by the use of crossed polarizers. One flash/frame was obtained by synchronization of the camera and strobe with a standard inverting circuit. The camera was triggered by a cable release mechanism so driven by a synchronous motor that it could yield exposures of single or multiple frames at intervals of 3, 6, or 15 s. Calibration runs made with $3 \times 10^{-3}$ m by $10^{-3}$ polyethylene disks established that the field of view of the camera encompassed approximately 5% of the solution volume.

In a typical experiment, crystallization was initiated by growing a single seed crystal into a subcooled solution out of the end of a hypodermic needle. The seeding system consisted of an inner hypodermic needle ($3 \times 10^{-4}$ m inside diam.) bonded with an epoxy resin at one end of a $0.64 \times 10^{-2}$ m O.D. plastic tube with the tip of the needle extending a short distance beyond the end of the tube (Figure 2a). The plastic tube could be inserted through the top lid and adjusted at any desired level facing the camera window. A flexible plastic tube through which Freon could be injected was inserted in the annulus between the hypodermic needle and plastic tube. Nucleation of the water in the hypodermic needle was initiated by spraying a small quantity of Freon in the lower portion of the annulus. Within a few seconds after spraying, a single crystal emerged at the tip of the needle. This method of introducing a seed crystal was initially developed with hopes that microscopic examination of the fixed crystal during a run would provide some insight on the mechanism of nucleation.

The only secondary nucleation observed, however, was that due to fracture of the seed crystal after it had grown to a size considerably larger than the average crystal size in continuous crystallizers. A fixed seed, produced by the method just described, does not simulate the behavior of a freely suspended crystal since it is subjected to different shear stresses and it cannot undergo crystal-impeller contact.

A second method of seeding the crystallizer was the injection of a piece of ice directly into the solution using the procedure illustrated in Figure 2b. A piece of ice, about 2 mm in diameter, was inserted through the side of a plastic probe onto the bottom ledge which had been chilled with dry ice. The other end of the plastic probe was connected to a nitrogen cylinder through a solenoid valve normally in the closed position. A plastic membrane was stretched across the crystallizer opening and the crystallizer conditions were adjusted to a desired level. A run was initiated by allowing the chilled probe to warm to a temperature at which the ice showed signs of surface melting, inserting the probe tip through the membrane across the crystallizer opening, sealing the crystallizer by tightening the cap about the probe, and displacing the seed crystal into the stirred crystallizer by a momentary opening of the solenoid valve.

The procedure for a typical experiment was as follows: after filling the crystallizer with the specified solution, the agitator was started and adjusted to the desired rotational speed. The movie camera was aimed at the glass window and focused on the tip of the hypodermic needle used for stationary seeding. At this time the refrigerant flow was started, rapidly chilling the contents of the crystallizer. The crystallizer pressure was adjusted to obtain the desired level of refrigerant subcooling at operating conditions. Eventually the temperature fell below the equilibrium freezing temperature and approached the desired level of subcooling. The refrigerant flow rate was then reduced to maintain the subcooling constant. The camera was started and the seed crystal introduced. This crystal nucleated new crystals which grew and in turn nucleated new crystals. Eventually, a large mass of crystals was formed and the temperature began to rise and in time reached the equilibrium freezing temperature.

## RESULTS AND DISCUSSION

Two types of data were obtained from each experiment; the number of crystals in an elemental volume of the crystallizer as a function of time from the movie film and the temperature versus time trace. A typical temperature versus time trace is shown in Figure 3. From such a plot the bulk subcooling may easily be determined from the difference between the initial temperature and the equilibrium freezing temperautre.

### Particle Count Data

Typical counts of crystals per frame are shown on a semilog scale in Figure 4 for two solution subcoolings. From Equation (7) the logarithm of the number of crystals per frame should be a linear function of time and the slope should be equal to the nucleation rate per crystal

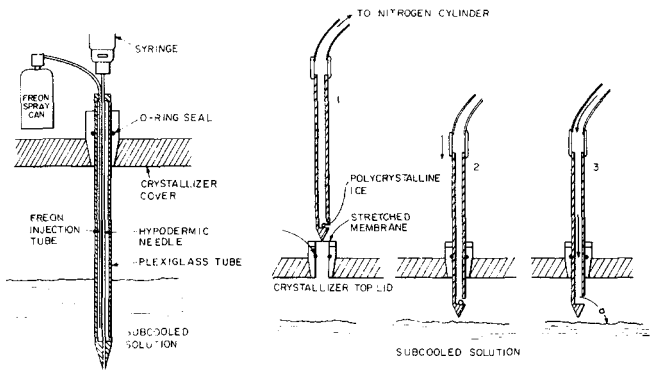


Fig. 2. Seeding techniques: (a) growth of seed crystal into subcooled solution, (b) injection of seed into solution.

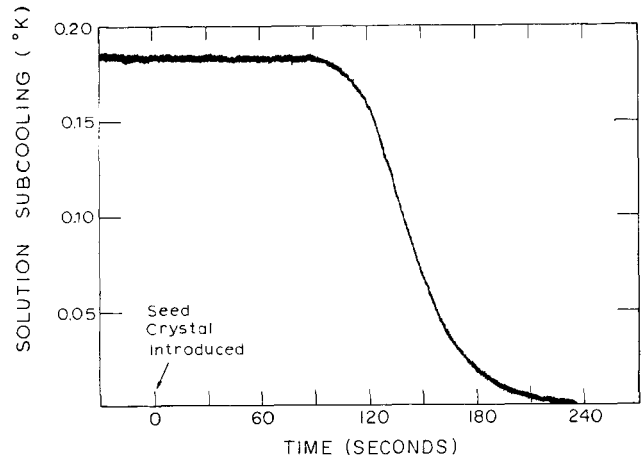


Fig. 3. Temperature-time relation for a 5.3 wt. % brine solution, a power input of 265 J/m$^3$s, and an initial subcooling of 0.186°K.

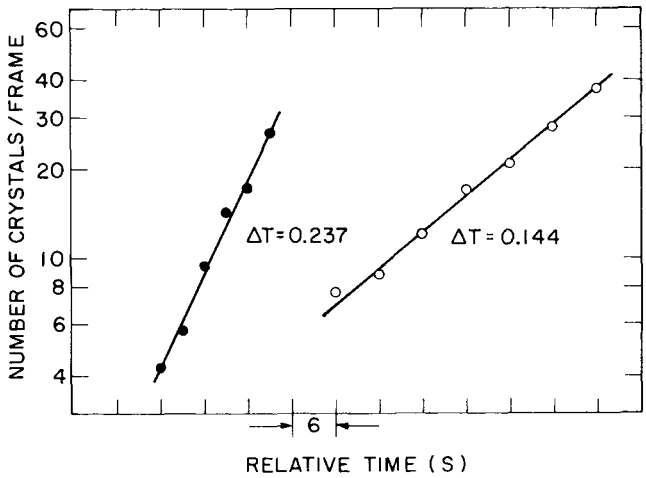


Fig. 4. Number of crystals vs. time for a 5.3 wt. % brine solution, an agitator power of 265 J/m$^3$s, and two solution subcoolings.

($\beta$). From the observed exponential growth of the number of crystals with time it can be inferred that the nucleation rate is proportional to the number of crystal present as assumed in the derivation of Equation (2).

### Temperature Data

The tedium of particle counting and the difficulty of obtaining good photographs at high agitation rates provided the motivation for developing a method of deducing $\beta$ from the temperature traces. From considerations of Equation (12) and temperature traces such as that shown in Figure 3, three alternative techniques were examined.

1. The temperature trace is reminiscent of chemical reactions with an induction period. This suggested the determination of $\beta$ from the time $I$, from the introduction of the seed crystal into the subcooled solution, required to reach a given arbitrary but small $(dT/dt)_c$. From Equation (12) one can show that $\beta$ can be obtained from $I$ and $(dT/dt)_c$ by solution of the following transcendental equation:

$$\beta I - 2 \ln \beta I = \ln \frac{(dT/dt)_c \rho C_p}{12 \pi \rho_I \lambda G_a^2 G_c I^2} + \ln \frac{n+1}{\mu_0^0 \left(1 + \sum_1^n \delta_k\right)} \quad (17)$$

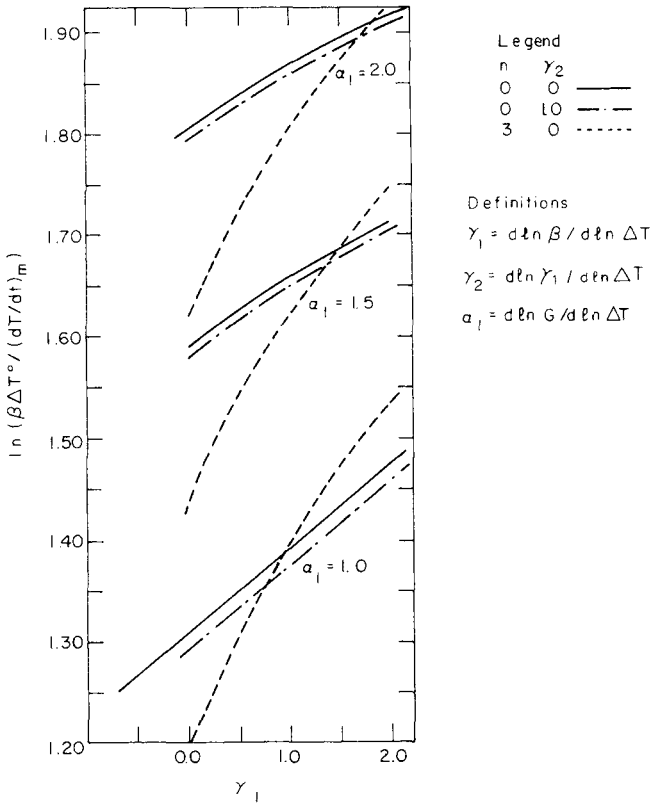


**Fig. 5. Effect of variations in $\alpha_1$, $\gamma_1$, and $\gamma_2$ on the calculated values of $\beta\,\Delta T^\circ/(dT/dt)_m$.**

The disadvantage of this method is that it requires knowledge of the growth rates $G_a$ and $G_c$, $n$, and the initial conditions in as much as they influence $\mu_0^0$ and $\delta_k$. It is also difficult to measure $(dT/dt)_c$ accurately.

2. In order to circumvent the problems associated with the use of Equation (17), Equation (12) can be integrated over a time interval for which the subcooling is sufficiently close to the initial value such that $G_a$, $G_c$, and $\beta$ can be treated as constants. Integration of Equation (12) from a time $t_1$ when the long time solution is valid, but the temperature is still essentially at its initial value to a time $t_2$ when the temperature has departed from its initial value by a measurable quantity, and division of the integral by the change in $(dT/dt)$ over the time interval yields

$$\frac{T(t_2) - T(t_1)}{(dT/dt)_{t_2} - (dT/dt)_{t_1}} = \frac{1}{\beta}$$

or, since $(dT/dt)_{t_1} << (dT/dt)_{t_2}$

$$\frac{(dT/dt)_{t_2}}{T(t_2) - T(t_1)} = \beta \qquad (18)$$

This method of determining $\beta$ has the advantage of not requiring knowledge of $n$, growth rates, or initial conditions. However, evaluation of the temperature difference $T(t_2) - T(t_1)$ and $(dT/dt)$ at a time $t_2$ when the subcooling is close to the initial value may be a source of significant error.

3. The characteristic feature of the temperature-time curve that is easiest to measure accurately is the maximum slope. Unfortunately, the maximum slope is observed at subcoolings appreciably different from the initial value, and it is therefore necessary in calculations of the slope to allow for the variations with subcooling of the growth rates and $\beta$. A method for calculating temperature traces numerically has been developed under the assumption that the ratio of the growth rates of the $a$ and $c$ axes is independent of subcooling. The analytical solutions for $\mu_0$, $\mu_1$, and $\mu_2$ are integrated over successive small time intervals using values of $G$ and $\beta$ evaluated for the temperature at the beginning of the interval. In the calculations it is further assumed that $G$ is proportional to $\Delta T^\alpha$, $\beta$ is proportional to $\Delta T^{\gamma_1}$, and $\gamma_1$ is proportional to $\Delta T^{\gamma_2}$. Numerous computer simulation runs were made for different values of $\beta$, $\alpha$, $\gamma_1$, $\gamma_2$, for values of $n$ from zero to three. The results are reported in Figure 5 and are applied here to the special case for which growth rates may be calculated using the approach of Brian, Hales, and Sherwood (1969) and, therefore, for which $\alpha$ is close to unity. For this case, the results of the numerical simulation runs support the following correlation between $\beta$ and the maximum derivative $(dT/dt)_M$ of the temperature-time plot:

$$\frac{\beta^0\,\Delta T^0}{(dT/dt)_M} = \exp\,[1.30 + 0.083\,\gamma_1] \qquad (19)$$

where $\Delta T^0$ is the initial subcooling and $\beta^0$ is the value of $\beta$ at the initial subcooling.

This method of determining $\beta$ depends on the knowledge of the sensitivity of $\beta$ and the crystal growth rate to the solution subcooling, but it is insensitive to the initial conditions, the absolute value of the growth rate, variations from 0 to 1 in $\gamma_2$, and, provided that $\alpha/\gamma_1$ is close to unity, to variations in $n$ from 0 to 3.

Since $\beta^0$ is approximately proportional to $(dT/dt)_M/\Delta T^0$, the value of $\gamma_1$ needed to derive $\beta$ from Equation (19) was obtained from the derivative of a curve fitted to log of $(dT/dt)_M/\Delta T^0$ vs. the log of $\Delta T^0$. The above procedure of obtaining $\beta$ yields a good match of the maximum slope in the temperature-time curve when the derived value of $\beta$ is used to calculate the entire temperature time distribution. The fit of the remainder of the temperature-time curve, shown for a representative run in Figure 6, gives a measure of confidence in the adequacy of the assumptions introduced in the calculations. A more critical check of the adequacy of the numerical simulation program is provided by the comparison shown in Figure 7 of the values of $\beta$ calculated from the maximum slopes

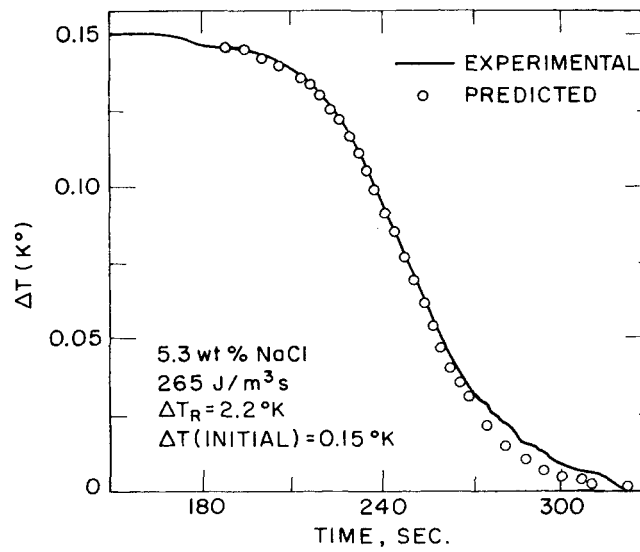


**Fig. 6. Comparison of predicted and experimental temperature time traces.**

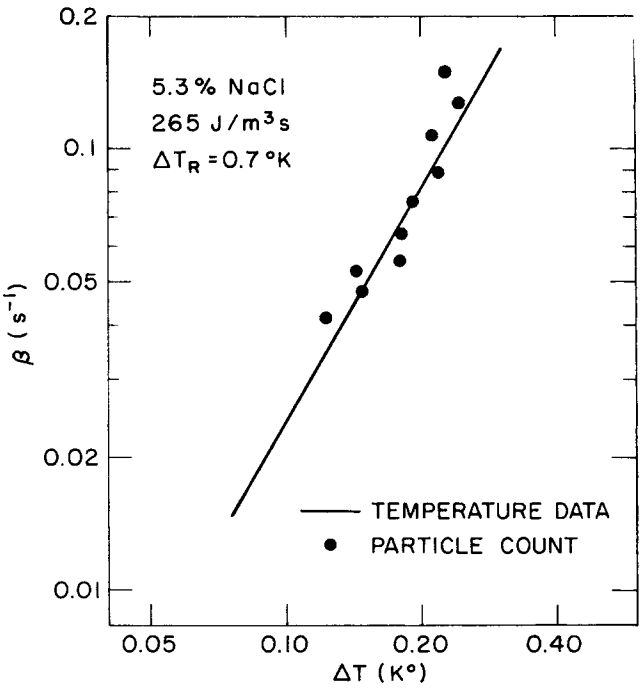


**Fig. 7. Comparison of nucleation rate obtained from temperature and optical measurements. Salt concentration = 5.3%, agitation power 265 J/m³s.**

with those obtained from the particle-count data. A stationary seed crystal was utilized to initiate crystallization in these experiments. The agreement between these two experimental techniques is excellent. The mean values agree within 7% and the power dependency on the solution subcooling within 12%. Both these values are within the scatter limits of the optical data.

When assessing these two experimental techniques three things should be considered. First, the time required to analyze the particle count data is orders of magnitude greater than that to analyze the temperature vs. time trace. Secondly, since the temperature trace experiment is much simpler than the optical experiment, the data for the former have much less scatter and are more precise. Finally, at higher agitation rates it is extremely difficult to obtain good photographs.

The differences in methods of measuring $\beta$ in continuous and batch crystallizers should be noted. In a continuous crystallizer the residence time ($= 1/\beta$) is fixed and the subcooling is measured, whereas in a batch experiment the initial subcooling is set and $\beta$ is inferred from either particle counts or the temperature versus time trace. For both the continuous and the batch experiment at long times ($\beta t > 2$ to 4 depending on the value of $n$) the measured nucleation parameter is $\beta$ and therefore it is not possible to determine $a_n$ and $n$. Since the $\delta_k$ function defined in Table 1 is a function of $n$, it is possible to infer $n$ in batch experiments from the initial transient if the size of the seed crystal is known.

Although the maximum slope was used in this paper to determine the nucleation parameter $\beta$, a method similar to the induction time has been employed in a recent study by Omran and King (1973). For the ice-brine system the temperature-time profile has been utilized; for other systems it may be more convenient to employ the concentration-time profile. This would require rewriting Equation (12) in terms of the concentration and applying Equation (19) to the concentration profile. In the most general sense the analysis is applicable to the supersaturation profile.


## ACKNOWLEDGMENT

The authors gratefully acknowledge the financial support provided by the Office of Saline Water of the Department of the Interior and many useful discussions with Dr. G. Margolis and Mr. A. Garcia.


## NOTATION

$a_n$ = nucleation rate constant, Equation (2)
$C_p$ = heat capacity per unit mass
$f$ = crystal size distribution
$G$ = crystal growth rate
$G_a$ = growth rate parallel to the basal plane
$G_c$ = growth rate normal to the basal plane
$h$ = crystal height
$I$ = induction time
$n$ = dependency of the actual nucleation rate ($\dot{N}$) on the crystal size
$\dot{N}$ = actual nucleation rate, Equation (2)
$r$ = characteristic dimension of the crystals, radius of the disk
$t$ = time
$T$ = temperature
$(dT/dt)_M$ = maximum slope of temperature profile
$\Delta T$ = bulk subcooling
$\Delta T_R$ = refrigerant subcooling
$V_c$ = volume of the crystals

### Greek Letters

$\beta$ = nucleation rate per crystal, Equations (6) and (16)
$\lambda$ = latent energy of fusion
$\rho$ = fluid density
$\rho_I$ = density of ice
$\tau$ = average residence time of crystals
$\mu_n$ = $n$th moment of crystal distribution

## LITERATURE CITED


Brian, P. L. T., H. B. Hales and T. K. Sherwood, "Transport of Heat and Mass Between Liquid and Spherical Particles in an Agitated Tank," *AIChE J.*, **15**, 727 (1969).

Evans, T. W., "Mechanisms of Secondary Nucleation during the Crystallization of Ice," Ph.D. thesis, Mass. Inst. Technol., Cambridge (1973).

Kane, S. G., "Secondary Nucleation of Ice in a Stirred Batch Crystallizer," Sc.D. thesis, Mass. Inst. Technol., Cambridge (1971).

Margolis, G., T. K. Sherwood, P. L. T. Brian, and A. F. Sarofim, "The Performance of a Continuous Well Stirred Ice Crystallizer," *Ind. Eng. Chem. Fundamentals*, **10**, 439 (1971).

Omran, A. M., and C. J. King, "Kinetics of Ice Crystallization in Sugar Solutions and Fruit Juices," paper presented at meeting of *AIChE*, New Orleans (1973).

Randolph, A. D., and M. A. Larson, *Theory of Particulate Processes*, Academic Press, New York (1971).


## APPENDIX. ANALYSIS OF A BATCH CRYSTALLIZER FOR SIZE DEPENDENT GROWTH

In the body of this paper it is shown that the particle size distribution of ice crystals growing in a batch crystallizer at constant subcooling becomes self-preserving after a short time. It is known, however, that the crystal growth rate is size dependent being governed by molecular diffusion and intrinsic growth kinetics at small sizes and by turbulent diffusion at larger sizes (see Brian et al., 1969; Margolis et al., 1971). In order to determine whether size dependent growth influences the conclusions drawn from the earlier calculations based on the assumption of constant growth rate, it is here assumed that the growth rate can be represented by

$$G = G_\infty (1 + x_0/r) \qquad \text{(A1)}$$

In the small particle limit Equation (A1) predicts a dependence of growth rate on size that would be expected for diffusion limited growth (neglecting any resistance due to limitations imposed by intrinsic kinetics). In the large particle limit, Equation (A1) predicts a size-independent growth rate as would be expected from the large particle asymptote of the correlations, reported by Brian et al. (1969), for heat and mass transfer to spheres in suspension. The large particle asymptote can be visualized as a regime in which the particle diameter is much larger than the scale of the eddies dominating the transfer process.

As before, the batch crystallizer is modeled assuming that:

1. $\dot{N} = a_n \mu_n$,
2. New crystals are nucleated at a size near zero, and
3. The batch crystallizer is seeded at time zero with a single crystal of small size.

Performing a balance on the $n$th moment (the nucleating moment) yields

$$\mu_n(t) = [r(t)]^n + \int_0^t [r(z)]^n \dot{N}(t-z)dz \qquad (A2)$$

where $r(t)$ is the size of a crystal at time $t$ which started at a size of zero at $t = 0$; that is,

$$r(t) = \int_0^t G[r(t')]\, dt'$$

Substituting

$$\psi_n(t) = [r(t)]^n$$

and using the first assumption transforms Equation (A2) into the following:

$$\mu_n(t) = \psi_n(t) + a_n \int_0^t \psi_n(z)\mu_n(t-z)dz \qquad (A3)$$

The Laplace transformation of Equation (A3) is

$$\mu_n(s) = \psi_n(s) + a_n \psi_n(s)\mu_n(s) \qquad (A4)$$

The solution for $\mu_n(s)$ is

$$\mu_n(s) = \frac{\psi_n(s)}{1 - a_n\psi_n(s)} \qquad (A5)$$

If the denominator of the transformed function defined by Equation (A5) has positive roots, the term of the solution for $\mu_n(t)$ corresponding to the largest positive root will dominate at long times. The roots of the denominator of the transformed function are defined by the equation:

$$1 = a_n \psi(s) \qquad (A6)$$

or

$$1 = a_n \int_0^\infty [r(t)]^n \exp(-st)dt$$

In proving that there exists a positive root for the general growth rate expressed by Equation (A1), it will first be shown that Equation (A5) has a positive root for both extreme cases (only small scale turbulence and only diffusion controlled heat and mass transfer). For the former case $r(t)$ is equal to $G_\infty t$ and therefore Equation (A6) has the following solution:

$$\beta = s = (a_n G_\infty{}^n n!)^{1/n+1}$$

If growth is diffusion controlled, $r(t)$ is equal to $(2x_0 G_\infty t)^{1/2}$ and the resulting positive root obtained from the solution of Equation (A6) is

$$\beta = s = \left[ a_n (2x_0 G_\infty)^{n/2} \Gamma\left(\frac{n}{2} + 1\right) \right]^{\frac{2}{n+2}}$$

Since there exists a positive root for both these extreme cases, it is inferred that there must also exist a positive root for the more general growth rate represented by Equation (A1).

The term of the solution for $\mu_n(t)$ corresponding to the largest positive root will dominate at long times and therefore the long time solution will have the form.

$$\mu_n(t) = k \exp(\beta t) \qquad (A7)$$

where $\beta$ is the maximum root and the nucleation parameter. Using the relationship,

$$f(r,t)\, G(r) = \dot{N}[t - \phi(r)] = a_n \mu_n(t - \phi(r))$$

and Equation (A7) it follows that

$$f(r,t) = a_n k \exp(\beta t)\left\{ \frac{\exp[-\phi(r)\beta]}{G(r)} \right\} \qquad (A8)$$

where $\phi(r)$ is the time required for a crystal to grow from zero size to $r$. From Equation (A8) the crystal size distribution is self-preserving and is defined by the size dependent part of the equation.

It has been shown for the case of size dependent growth that the crystal size distribution becomes self-preserving at long times and therefore there exists a unique nucleation parameter $\beta$. It only remains to verify that $\beta$ is identical to the inverse of the residence time for a continuous crystallizer.

A population balance for a continuous crystallizer at steady state is as follows:

$$\frac{\partial z}{\partial r} = \frac{-z}{G(r)\tau} \qquad (A9)$$

where $z$ is equal to $G(r)f(r)$. The term on the left represents the number of crystals growing into the size range ($r$ to $r + dr$) less the number growing out of the size range, while the term on the right is the number of crystals in this range which are removed from the crystallizer. Solving Equation (A9) for $z$ yields

$$z = z_0 \exp\left\{ -\int_0^r \frac{dr'}{G(r')\tau} \right\} \qquad (A10)$$

where

$$z_0 = (fG)_{r=0} = \dot{N}$$

Solving Equation (A10) for $f(r)$ results in the following relationship:

$$f(r) = \frac{\dot{N}}{G(r)} \exp\left\{ \frac{-\phi(r)}{\tau} \right\} \qquad (A11)$$

where $\phi(r)$ again represents the time for a crystal to grow to a size $r$. From the crystal size distribution Equation (A11) and the definition of the $m$th moment the $m$th moment can be expressed as

$$\mu_m = \dot{N} \int_0^\infty r(\phi)^m \exp\left\{ \frac{-\phi}{\tau} \right\} d\phi \qquad (A12)$$

For the special case of $m$ equal zero Equation (A12) has the solution

$$\mu_0 = \dot{N}\tau = a_n \mu_n \tau \qquad (A13)$$

Utilizing Equations (A12) and (A13) results in the following relationship for the inverse residence time:

$$\frac{1}{\tau} = \frac{a_n \mu_n}{\mu_0} = \frac{a_n}{\tau} \int_0^\infty r(\phi)^n \exp\left\{ \frac{-\phi}{\tau} \right\} d\phi \qquad (A14)$$

Finally after a minor simplification the following equation is obtained

$$1 = a_n \int_0^\infty r(\phi)^n \exp\left\{ \frac{-\phi}{\tau} \right\} d\phi \qquad (A15)$$

Equation (A15) is identical to Equation (A6) except the inverse of the residence time ($1/\tau$) has replaced $s$ or $\beta$. Since Equation (A6) defines $\beta$ and Equation (A15) can be thought of as defining $1/\tau$, then $\beta$ must equal $1/\tau$. As can be seen from Equation (A13) for the case of size dependent growth $1/\tau$ is again equal to the nucleation rate per crystal and therefore $\beta$ can be defined as the nucleation rate per crystal.

In conclusion, irrespective of the dependency of the growth rate on the crystal size, the crystal size distribution will become self-preserving at long times and therefore a unique value of $\beta$ will exist. Furthermore, $\beta$ will be numerically equal to the inverse of the average residence time for a continuous crystallizer and is equivalent to the nucleation rate per crystal.

*Manuscript received November 9, 1973; revision received and accepted April 8, 1974.*